Structural and optical properties of single crystal $Zn_{1-x}Mg_xO$ nanorods—Experimental and theoretical studies

Yu-Sheng Chang, Chih-Tao Chien, and Chun-Wei Chen[a)]
Department of Materials Science and Engineering, National Taiwan University, Taipei, Taiwan

Ta-Ya Chu
Institute and Department of Electrophysics, National Chiao-Tung University, Taiwan

Hsuen-Han Chiang, Chen-Hao Ku, and Jih-Jen Wu
Department of Chemical Engineering, National Cheng Kung University, Tainan, Taiwan

Chao-Sung Lin
Department of Materials Science and Engineering, National Taiwan University, Taipei, Taiwan

Li-Chyong Chen
Center for Condensed Matter Sciences, National Taiwan University, Taipei, Taiwan

Kuei-Hsien Chen
Institute of Atomic and Molecular Sciences, Academic Sinica, Taipei, Taiwan

(Received 5 June 2006; accepted 13 November 2006; published online 1 February 2007)

Structural and optical properties of single crystal $Zn_{1-x}Mg_xO$ nanorods ($0 \leq x \leq 0.17$) are studied experimentally and theoretically. Structural analyses indicate that the nanorods grown on Si substrates are oriented in the *c*-axis direction and the nanorods possess the single-crystalline hexagonal structure with the Mg incorporated within the ZnO nanorods by means of substituting Zn. A blueshift of the near-band edge emission in the photoluminescence spectra by increasing Mg content is observed. Two distinct emission bands are found in the photoluminescence spectra; one is mainly attributed to the delocalized exciton recombination and the other is originating from localized excitons due to the incorporation of foreign impurity of Mg. Enhanced exciton localization with increasing Mg content in $Zn_{1-x}Mg_xO$ nanorods is mainly due to large ionic characters of Mg-O bonding. Structural stability, band structures, projected density of states, and charge distribution in various $Zn_{1-x}Mg_xO$ alloy compounds were further investigated by first-principles calculations. A good agreement between experimental and theoretical results is found. © *2007 American Institute of Physics*. [DOI: 10.1063/1.2429729]

I. INTRODUCTION

ZnO has a direct band gap of 3.37 eV with a large exciton binding energy of 60 meV at room temperature. Due to the strong binding energy of excitons, ZnO-based semiconductors are recognized as very promising photonic materials in the ultraviolet (UV) region.[1,2] Room-temperature UV lasing properties in ZnO epitaxial films,[3] microcrystalline thin films,[4] and nanoclusters[5] have been successfully demonstrated. Recently, the research on one-dimensional well-aligned single crystalline ZnO nanorods has attracted considerable attention owing to their potential applications in nanoscale optoelectronic devices.[6] Two critical challenges in fabricating ZnO laser diodes are *p*-type doping and band gap engineering in alloy semiconductors to create barrier layers and quantum wells which facilitate radiative recombination by carrier confinement. The addition of impurities among the wide band gap semiconductors often induces dramatic changes in their structural and optical properties. For example, ternary $Zn_{1-x}Cd_xO$ alloy has an energy gap lower than that for ZnO to serve as an active layer for light emission in the visible range because of the smaller direct band gap of CdO of 2.3 eV.[7] The value of the energy gap of ternary $Zn_{1-x}Be_xO$ can be efficiently engineered to values larger than ZnO due to the larger band gap of BeO (10.6 eV).[8] $Zn_{1-x}Mg_xO$ is another candidate to develop ZnO-based alloy that has an energy gap larger than that of ZnO. The optical band gap energies of the hexagonal $Zn_{1-x}Mg_xO$ films are tunable from 3.3 to 4.0 eV at room temperature as the content of Mg is increased upward to $x=0.33$.[9]

Since the crystal structures of ZnO and MgO are wurtzite (hexagonal, $a=3.24$ Å and $b=5.20$ Å) and rock salt (cubic, $a=4.24$ Å), respectively, the solubility limit of Mg in ZnO depends on the growth mechanisms as well as growth conditions.[10–12] Alloying ZnO with the increasing concentration of Mg can lead to structural evolution from a hexagonal phase to a cubic phase. Recently, one-dimensional $Zn_{1-x}Mg_xO$ nanorods have been synthesized and tunable photoluminescence (PL) emission with Mg content can be achieved.[13] A blueshift of the near-band edge emission with increasing Mg content is observed, indicating the $Zn_{1-x}Mg_xO$ nanorods can be used as an excellent band gap engineering material for near UV nanophotonic applications. In this article, temperature and power dependent photoluminescence measurements were employed to investigate the

[a)]Author to whom correspondence should be addressed; electronic mail: chunwei@ntu.edu.tw

fundamental optical properties of $Zn_{1-x}Mg_xO$ ($0 \leq x \leq 0.17$) nanorods. In addition, a comprehensive study of structural and optical properties in alloy $Zn_{1-x}Mg_xO$ compounds by first-principles calculations is also presented.

II. EXPERIMENTAL SETUP AND CHARACTERIZATIONS

Highly oriented $Zn_{1-x}Mg_xO$ nanorods were prepared on a Si(100) substrate by catalyst-free metalorganic chemical vapor deposition at low temperature of 500 °C. The fabrications of the $Zn_{1-x}Mg_xO$ nanorods were detailed elsewhere.[13] In brief, tuning the partial pressures of the Zn and the Mg sources in gas phase via adjusting the vaporizing temperatures of the Zn and the Mg sources as well as the diameters of the Zn and the Mg source containers were employed to tailor the Mg contents of the single phase $Zn_{1-x}Mg_xO$ nanorods grown in the metalorganic chemical vapor deposition reactor. Zinc and magnesium metalorganic sources, zinc acetylacetonate $[Zn(C_5H_7O_2)_2$, Lancaster, 98%] and magnesium acetylacetonate $[Mg(C_5H_7O_2)_2$, Aldrich, 98%], which were placed in two Pyrex glass containers were loaded into the two low-temperature zones of the furnace where the temperatures are controlled in the range of 115–125 and 185–215 °C, respectively. The morphology of the nanorods was examined using scanning electron microscopy (SEM) (Hitachi, S-4200). Elemental analyses were conducted using the electron probe x-ray microanalyzer (EPMA) (JOEL, JXA-8600SX). The crystal structures of the $Zn_{1-x}Mg_xO$ nanorods were investigated by x-ray diffraction (XRD) (Rigaku D/MAX-2000) and transmission electron microscopy (TEM) (JOEL 2010).The PL spectra were obtained by exciting the samples using a continuous wave He-Cd laser (325 nm) and the emission spectra were analyzed with a Jobin–Yvon TRIAX 0.55 m monochromator and detected by a photomultiplier tube and standard photocounting electronics. The samples were maintained under vacuum inside a helium cryostat during measurements.

III. COMPUTATIONAL METHOD

The calculations were performed using first-principles, plane-wave, pseudopotential approach within the framework of density-functional theory (DFT) implemented in the CASTEP codes.[14] The exchange-correction functional is approximated by the local-density approximation (LDA). The ion-electron interaction is modeled by the nonlocal, norm conserving pseudopotential.[15] The summation over the Brillouin zone was carried out with a *k*-point sampling using a Monkhorst–Pack grid.[16] Ten different cubic and hexagonal derived $Zn_{1-x}Mg_xO$ structures with different compositions (x=0, 0.25, 0.5, 0.75, and 1, respectively) are used to study the energetic stabilities and electronic structures. A kinetic-energy cutoff of 280 eV and 25 special *k* points were used to ensure the convergence in the calculations. In searching for the lowest-energy geometries for these crystals, each structure was optimized for a specified cell geometry with relaxation of both lattice parameters and atomic positions.

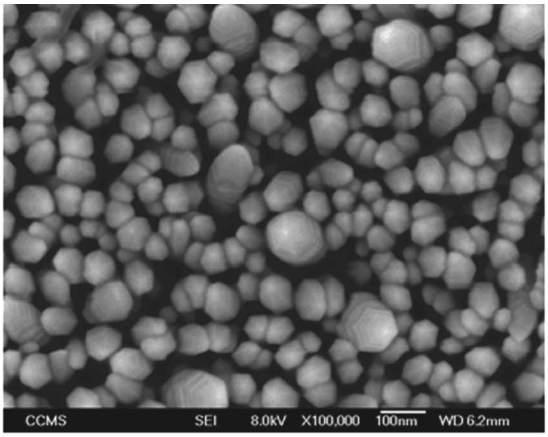

(a)

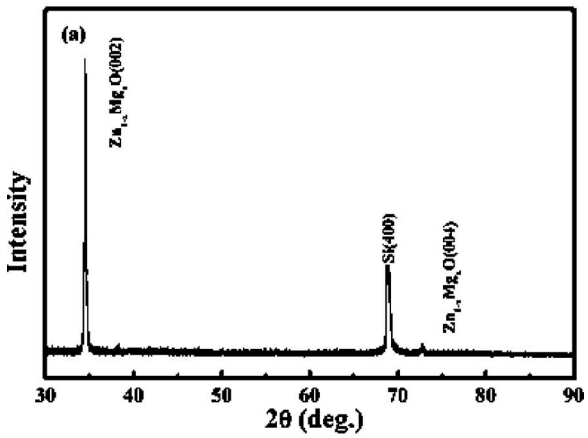

(b)

FIG. 1. (a) SEM micrograph of the well-aligned $Zn_{1-x}Mg_xO$ nanorods. (b) Typical XRD pattern of the $Zn_{1-x}Mg_xO$ nanorods (x=0.10).

IV. RESULTS AND DISCUSSION

A. Experimental results

1. Structural properties

Figure 1(a) depicts the SEM image of the formation of a high density of well-aligned $Zn_{1-x}Mg_xO$ nanorods. According to EPMA measurement, Mg content of $Zn_{1-x}Mg_xO$ nanorods is tunable from 0 to 0.17 by adjusting the partial pressures of the Zn and Mg sources in gas phase. A typical XRD pattern of the well aligned $Zn_{1-x}Mg_xO$ nanorods is shown in Fig. 1(b). In addition to the Si(004) diffraction peak, a peak very closed to (002) diffraction peak of the hexagonal (wurtzite) ZnO structure appearing in the pattern implies that $Zn_{1-x}Mg_xO$ nanorods possess the same structure as that of the ZnO and they preferentially orient in the *c*-axis direction. There is no diffraction peak of MgO or Mg crystal present in the XRD pattern. The *c*-axis lattice constants calculated from the *d* (002) peaks for the $Zn_{1-x}Mg_xO$ nanorods show a decreasing function of the Mg concentration as shown in Table I. The obtained *c*-axis lattice constant of ZnO nanorods (5.1962 Å) is less than the previous report (5.206 Å),[17] which may results from the possible origin of stress in our samples due to the smaller diameters (50–80 nm) com-

TABLE I. The lattice constant (c axis), exciton band gap, and FHWM for $Zn_{1-x}Mg_xO$ nanorods with x=0, 0.03, 0.07, 0.10, and 0.17, respectively.

	ZnO	$Zn_{1-x}Mg_xO$ (x=0.03)	$Zn_{1-x}Mg_xO$ (x=0.07)	$Zn_{1-x}Mg_xO$ (x=0.10))	$Zn_{1-x}Mg_xO$ (x=0.17)
Lattice constant c axis (Å)	5.1962	5.1961	5.1914	5.1889	5.1834
Exciton band gap (eV) at 25 K	3.376 (X_A) 3.382 (X_B) 3.365 (D^0X1) 3.360 (D^0X2)	3.427 (B) 3.412 (L)	3.484 (B) 3.463 (L)	3.537 (B) 3.508 (L)	3.645 (B) 3.606 (L)
FHWM (meV) at 25 K					
Total	2.54 (D^0X2)	32.1	45.4	65.1	89.9
B band	···	12.8	19.0	20.0	51.0
L band	···	20.5	26.0	44.5	56.2

pared to those in the Ref. 17 (~300 nm). In addition, the increasing surface-to-volume ratio with decreasing diameters in ZnO nanorods could also account for shortening of the c-axis lattice constant according to the theoretical calculations,[18] where the contraction of the in-plane Zn-O bond length occurs in the ZnO nonpolar $[10\bar{1}0]$ surface. Further structural characterizations of the well-aligned $Zn_{1-x}Mg_xO$ nanorods were performed using the TEM analysis. A cross-sectional TEM image of the $Zn_{1-x}Mg_xO$ (x =0.10) nanorods on the Si substrate as shown in Fig. 2(a) demonstrates that most of the nanorods were grown perpendicularly to the substrate. The corresponding selected area diffraction (SAD) of the cross-sectional image is illustrated in the inset. All the d spacing values estimated from the SAD are consistent with those of the ZnO structure and are mismatching with those of the MgO and the Mg structures, confirming the XRD analyses that MgO and Mg phases are not observed in the nanorods. Figure 2(b) illustrates a typical high-resolution (HR) TEM image of the $Zn_{1-x}Mg_xO$ nanorod as well as the corresponding electron diffraction pattern. The lattice spacing of around 0.52 nm corresponds to the d spacing of (001) crystal planes of the hexagonal ZnO. No segregated cluster of impurity phase appears throughout the nanorod via HRTEM observation. The absence of the diffraction peaks of MgO or Mg phase in the XRD and TEM patterns and the systematic dependence of the Mg content with the lattice constant both imply that the Mg incorporated within the ZnO nanorods by means of substituting Zn.

2. Optical properties

Figure 3 shows the low temperature PL spectra of $Zn_{1-x}Mg_xO$ nanorods measured at 25 K with x equal to 0, 0.03, 0.07, 0.10, and 0.17, respectively. First, a blueshift of the near-band edge emission with increasing Mg content is observed. For the undoped ZnO nanorods, several sharp peaks in the vicinity of the band edge are observed. The inset exhibits the near-band edge emission of the ZnO nanorods consisting of four distinct peaks at 3.360, 3.365, 3.376, and 3.382 eV, respectively. The PL emission peaks at 3.376 and 3.382 eV are attributed to free A and B excitons and the peak positions at 3.365 and 3.360 eV are ascribed to neutral bound exciton peaks D^0X1 and D^0X2, respectively, in a good agreement with the reported values in ZnO epilayers[19] and nanorods.[17] The green band at ~2.5 eV caused by the intrinsic defects or oxygen vacancies in the ZnO (Refs. 20 and 21) is almost negligible, implying that the ZnO nanorods are almost defect free and of high quality. The full half width maximum (FHWM) value of the D^0X2 exciton peak for ZnO

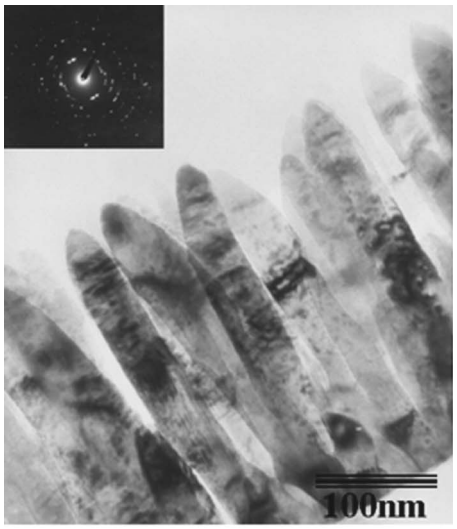

(a)

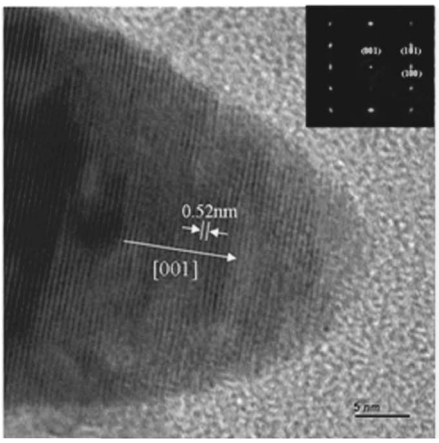

(b)

FIG. 2. (a) TEM cross-sectional image of $Zn_{1-x}Mg_xO$ nanorods (x=0.10) and SAD pattern (inset). (b) High-resolution TEM image of the top region of an individual $Zn_{1-x}Mg_xO$ nanorod (x=0.10) and the corresponding electron diffraction pattern (inset).

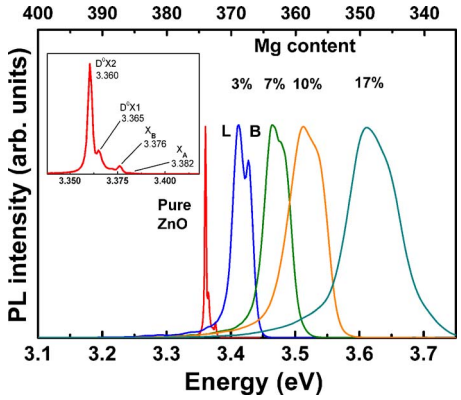

FIG. 3. PL spectra for $Zn_{1-x}Mg_xO$ nanorods with $x=0$, 0.03, 0.07, 0.10, and 0.17 measured at 25 K. The inset shows the details of the near-band edge region of ZnO nanorods.

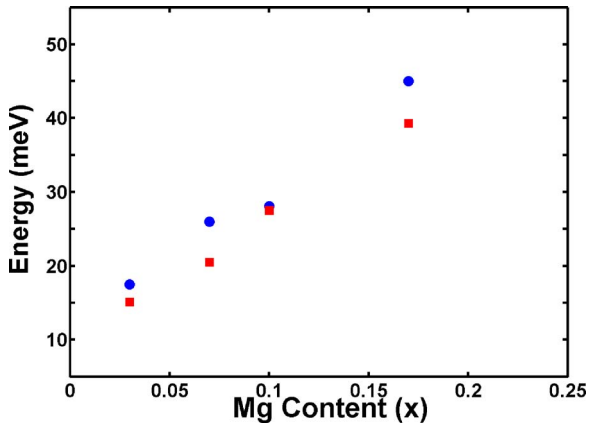

FIG. 5. Correlation of thermal activation energy E_a of the L band emission (circle) and the energy separation E (square) at 25 K between bands B and L for $Zn_{1-x}Mg_xO$ nanorods with $x=0.03$, 0.07, 0.10, and 0.17, respectively.

nanorods is about 2.5 meV, which is as narrow as those for bulk crystals.[3] The increasing FHWM value with Mg content in $Zn_{1-x}Mg_xO$ nanorods is associated with alloy broadening commonly observed in alloy semiconductors. The PL spectra for $Zn_{1-x}Mg_xO$ nanorods can be further fitted with two Lorentzian functions labeled as B and L bands, respectively. The B band emission has a higher energy than the L band emission. The results are summarized in Table I

In order to understand the fundamental properties of B and L emission bands, a series of temperature- and power-dependent PL measurements were carried out. Figure 4 shows the evolution of PL spectra of $Zn_{1-x}Mg_xO$ nanorods with $x=0.03$, 0.10, and 0.17, respectively, measured from 25 K to room temperature. A clear evolution from band L to band B is found when temperature is increased. For $x=0.03$, band L is quickly thermally quenched and becomes unnoticeable at temperatures above 75 K. These transition temperatures are 200 and 250 K for $x=0.10$ and 0.17, respectively. The distinct character of L band emission can observed at a higher temperature with increasing Mg content, leading to the assignment of the L band emission originating from excitons being localized by the foreign impurity of Mg atoms. The disorder and fluctuation is larger in ZnO than in III–V semiconductors because excitons in ZnO have a small Bohr radius (18 Å) and are more sensitive to local inhomogeneity.[22] Figure 5 shows the correlation of the thermal activation energy E_a of the L band emission and the energy separation E at 25 K between bands B and L for $Zn_{1-x}Mg_xO$ nanorods ($0 \leq x \leq 0.17$). As the Mg content is increased, the excitonic localization is enhanced and the energy separation E between bands B and L is also increased. At higher temperature, band L is thermally quenched and the localized excitons are dissociated into the delocalized excitons.

Figure 6(a) shows the excitation power dependence of PL spectra for the $Zn_{1-x}Mg_xO$ nanorod sample ($x=0.03$) at 25 K. There is no shift in the emission peak positions for B and L bands over the whole excitation energy range. As the excitation power <4.5 mW, the intensity of L emission band is larger than B emission band. With the increase of excitation power >4.5 mW, the predominant B emission band is observed. The integrated PL intensity of the B emission band increases linearly with excitation power; in contrast, the intensity of the L emission band reaches to saturation as the excitation power >4.5 mW. The situation is very different for the $Zn_{1-x}Mg_xO$ nanorods with higher Mg content. Figure 6(b) shows the excitation dependent PL spectra for the $Zn_{1-x}Mg_xO$ nanorods with $x=0.10$. The integrated PL intensities for both B and L emission bands exhibit a monotonic increasing function with excitation power. More pronounced L band emission is always observed over the whole excitation range. For the $Zn_{1-x}Mg_xO$ nanorods with low Mg content ($x=0.03$), the photogenerated excitons are no longer able to be localized by Mg-related sites as the excitation power >4.5 mW, leading to the saturation of L band emission in-

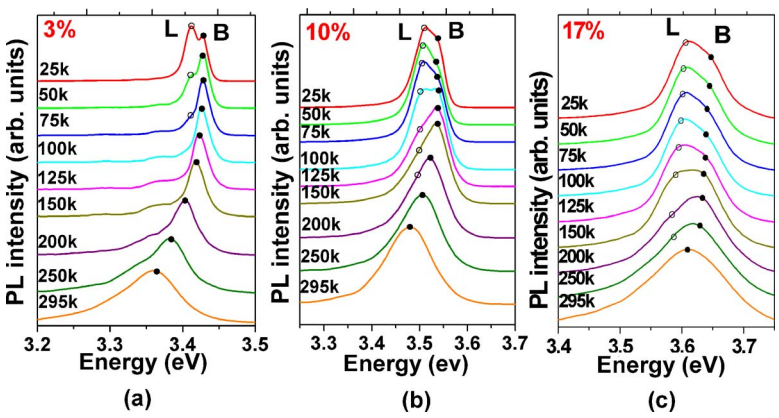

FIG. 4. Temperature dependent of PL spectra for $Zn_{1-x}Mg_xO$ nanorods with (a) $x=0.03$, (b) $x=0.10$, (c) $x=0.17$, respectively. The filled circle (●) represents the B band emission and the open circle (○) represents the L band emission, respectively.

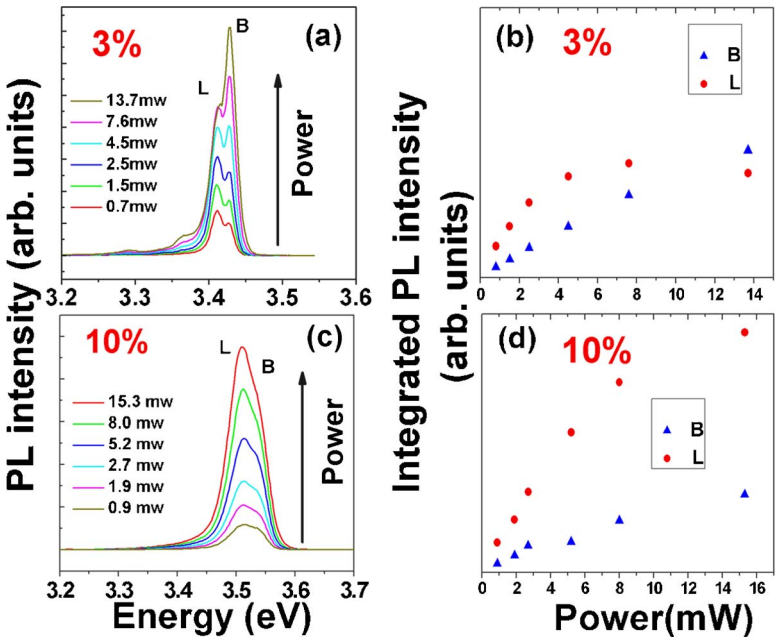

FIG. 6. Excitation power dependence of PL spectra measured at 25 K for $Zn_{1-x}Mg_xO$ nanorods with (a) $x=0.03$ and (c) $x=0.10$, respectively. Plots of the integrated intensities of B and L emission varying with excitation power (b) for $x=0.03$ and (d) for $x=0.10$, respectively.

tensity. Further increase in excitation power predominantly prompts the emerging emission related to delocalized excitons. For the $Zn_{1-x}Mg_xO$ nanorods with $x=0.10$ which consists of a higher population of Mg atoms, the photogenerated excitons are predominantly localized to the impurities of Mg atoms within our excitation power range. The earlier results indicate that B band emission is mainly attributed to the delocalized exciton recombination and the L band emission is originating from localized exciton recombination due to the incorporation of foreign impurity of Mg. Similar observation has also been reported in the GaNAs/GaAs quantum well structure.[23] It is worth noting that no stimulated emission or biexciton emission as seen in ZnO nanorods[17] is expected due to the relatively low excitation power in our measurements.

B. Theoretical simulations

1. Structural properties

Ohtomo *et al.*,[9] who obtained $Zn_{1-x}Mg_xO$ alloys with a hexagonal phase up to $x=0.36$, beyond which MgO phase separation started to occur. Chen *et al.*[24] have summarized approximately the dependence of Mg concentration on the band gap energy in $Zn_{1-x}Mg_xO$ thin films for x varying from 0 to 82 at. % and indicate that the hexagonal structure is more favorable for $x<0.4$, and the cubic phase is more stable for $x>0.6$. There is a mixed hexagonal and cubic phase for Mg content between 37% and 62%. Figure 7 exhibits the relative structural stability of ten different optimized hexagonal and cubic $Zn_{1-x}Mg_xO$ crystals with different Mg content ($x=0$, 0.25, 0.50, 0.75, and 1.0). From the total energy calculations, it is found that the hexagonal $Zn_{1-x}Mg_xO$ crystal is energetically favorable compared to the cubic-phase $Zn_{1-x}Mg_xO$ crystal for $x<0.7$. Our simulated results account for the structural stability of hexagonal and cubic $Zn_{1-x}Mg_xO$ crystals based on their electronic structures where no thermodynamic factor (0 K) is considered during calculations. Therefore, the discrepancy between the simulated and experimental results for $0.4\leq x\leq 0.6$ is expected, where a mixed hexagonal and cubic phase exists. According to the phase diagram of ZnO-MgO binary systems, the thermodynamic solid solubility of MgO in a ZnO matrix is normally less than 4 at. %.[25] The enhancement of solubility limit of $Zn_{1-x}Mg_xO$ might be explained in terms of nonthermal equivalent nature during different growth conditions. The variations of lattice constants a and c of simulated hexagonal $Zn_{1-x}Mg_xO$ crystals with increasing Mg content are shown in Table II. As Zn is replaced by Mg in the ZnO crystal ($Zn_{0.75}Mg_{0.25}O$), although the ionic radius of Mg^{2+} (0.57 Å) is smaller than Zn^{2+} (0.60 Å),[26] the Mg-O bond length along the c axis is enlarged from 1.997 to 2.009 Å due to the nature of more ionic Mg-O bonding. However, the buckled hexagonal rings of the wurtzite basal plane ($\perp c$ axis) become flat with increasing Mg content (from 108.72° to 108.22°). As a result, the a-axis length in the lattice gradually increases, while the c-axis length decreases with increasing Mg content, consistent with our experimental results and also with other $Zn_{1-x}Mg_xO$ films.[9]

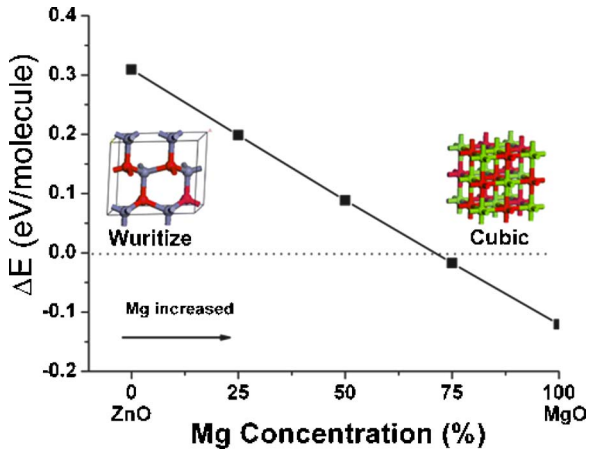

FIG. 7. Relative structural stability of simulated hexagonal and cubic $Zn_{1-x}Mg_xO$ crystals with $x=0$, 0.25, 0.50, 0.75, and 1, respectively.

TABLE II. The variation of lattice constants a and c of simulated hexagonal $Zn_{1-x}Mg_xO$ crystals with increasing Mg content.

x	0%	25%	50%	75%	100%
a (Å)	3.275	3.297	3.313	3.325	3.333
c (Å)	5.270	5.248	5.221	5.203	5.175

2. Electronic structure calculations

The alloy band gap bowing behavior in hexagonal $Zn_{1-x}Mg_xO$ crystals is also examined. The experimental gap of ZnO is 3.37 eV and a band gap correction parameter of 2.42 eV is required for our calculations due to the underestimation of band gap by LDA. With the correction applied to all other hexagonal $Zn_{1-x}Mg_xO$ crystals, we obtain a bowing coefficient b of 0.72 eV for these compounds, defined as

$$E_g(x) = 3.37(1-x) + 5.91x - bx(1-x), \quad (1)$$

where 3.37 and 5.91 eV are the band gap values of hexagonal ZnO and MgO crystals, respectively, after band gap correction. Figure 8 shows the variation of band gap with Mg content in hexagonal $Zn_{1-x}Mg_xO$ crystals with $0 \le x \le 0.45$ by Eq. (1) in comparison with experimental results. A good consistency between the theoretical and experimental results for $x < 0.25$ is found. For $x > 0.3$, the discrepancy between the experimental and simulated results may be attributed to the mixed phase in this region from experimental results.

Large exciton localization effect in $Zn_{1-x}Mg_xO$ nanorods with increasing Mg content can be further realized by the following electronic structure calculations. Figures 9(a) and 9(b) show the partial density of states (PDOS) of O $2p$ and Zn $3d$ bands of hexagonal $Zn_{1-x}Mg_xO$ ($x=0$, 0.25, and 0.5) crystals, respectively. It is clearly shown that both O $2p$ and Zn $3d$ bands become more localized in the top of valence bands with a narrower bandwidth and larger PDOS intensity as the Mg content increases. The enhanced localization in O $2p$ and Zn $3d$ bands indicates that more ionic characters in $Zn_{1-x}Mg_xO$ crystals are found with increasing Mg content.

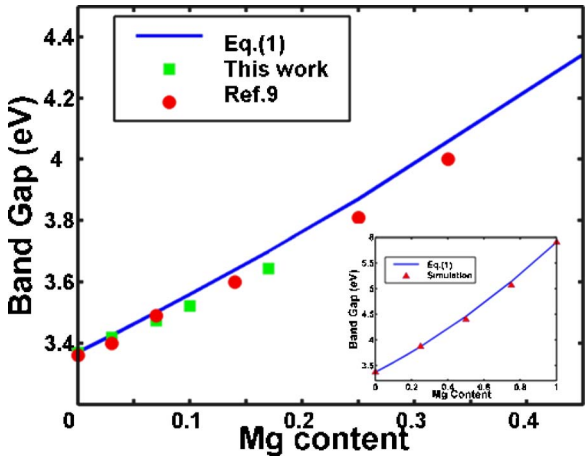

FIG. 8. Variations of band gap values in hexagonal $Zn_{1-x}Mg_xO$ crystals with $0 \le x \le 0.45$ by Eq. (1) (line) in comparison with experimental results of Ref. 9 (circle) and this experimental work (square). The inset shows the variation of band gap of the simulated hexagonal $Zn_{1-x}Mg_xO$ crystal structures (triangle) with $x=0$, 0.25, 0.50, 0.75, and 1 with respect to the Eq. (1) (line).

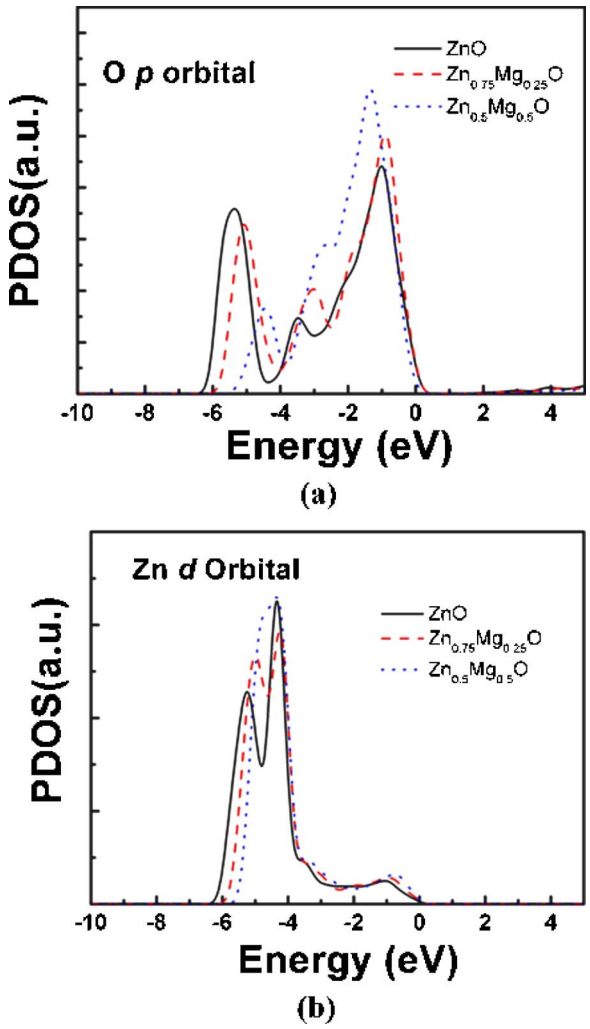

FIG. 9. PDOS of (a) O $2p$ and (b) Zn $3d$ bands in hexagonal $Zn_{1-x}Mg_xO$ crystals ($x=0$, 0.25, and 0.5), respectively. The 0 eV is defined as the top of the valence band.

As a result, the photogenerated excitons will be localized more effectively in $Zn_{1-x}Mg_xO$ crystals with increasing Mg content, which accounts for the distinct characters between L and B band emission in our experiments.

V. CONCLUSION

In conclusion, we have investigated the structural and optical properties in $Zn_{1-x}Mg_xO$ nanorods experimentally and theoretically, by temperature and power dependent PL spectra and first-principles calculations. The structural and optical properties in $Zn_{1-x}Mg_xO$ nanorods can be tuned by varying the Mg content. Although the Mg-O bond length along the c axis is increased in $Zn_{1-x}Mg_xO$ crystals, the buckled hexagonal rings of the wurtzite basal plane become flat with increasing Mg content. As a result, the a-axis length in the lattice gradually increases, while the c-axis length decreases. A blueshift of the near-band edge emission with increasing Mg content is observed and can be well described by a bowing equation from our calculations. Two distinct emission B and L bands are found in the PL spectra. The B emission band is mainly attributed to the delocalized exciton recombination. The L band emission originating from local-

ized excitons is largely enhanced with increasing Mg content in $Zn_{1-x}Mg_xO$ crystals due to their more ionic features.

ACKNOWLEDGMENT

This work is supported by National Science Council, Taiwan. (Project Nos. NSC94–2120-M-001–015, NSC94–2112-M-002–040, and NSC95–2120-M-002–014).

[1]H. J. Ko and Y. F. Chen, Z. Zhu, T. Yao, I. Kaobayyashi, and H. Uchiki, Appl. Phys. Lett. **76**, 1905 (2000).
[2]W. I. Park, Y. H. Jun, S. W. Jung, and G.-C. Yi, Appl. Phys. Lett. **82**, 964 (2003).
[3]D. M. Bagnall, Y. F. Chen, Z. Zhu, T. Yao, S. Koyama, M. Y. Shen, and T. Goto, Appl. Phys. Lett. **70**, 2230 (1997).
[4]P. Zu, Z. K. Tang, G. K. L. Wong, M. Kawasaki, A. Ohtomo, H. Koinuma, and Y. Segawa, Solid State Commun. **103**, 459 (1997).
[5]H. Cao, J. Y. Xu, E. W. Seelig, and R. P. H. Chang, Appl. Phys. Lett. **76**, 2997 (2000).
[6]M. H. Huang *et al.*, Science **292**, 1897 (2001).
[7]T. Gruber *et al.*, Appl. Phys. Lett. **83**, 3290 (2003).
[8]Y. R. Ryu *et al.*, Appl. Phys. Lett. **88**, 052103 (2006).
[9]A. Ohtomo *et al.*, Appl. Phys. Lett. **72**, 2466 (1998); The band gap values used in the text are obtained from the inset in Fig. 4 of Ref. 9.
[10]S. Choopun, R. D. Vispute, W. Yang, R. P. Sharma, T. Venkatesan, and H. Shen, Appl. Phys. Lett. **80**, 1529 (2002).
[11]W. I. Park, G.-C. Yi, and H. M. Jang, Appl. Phys. Lett. **79**, 2022 (2001).
[12]A. K. Sharma, J. Narayan, J. F. Muth, C. W. Teng, C. Jin, A. Kvit, R. M. Kolbas, and O. W. Holland, Appl. Phys. Lett. **75**, 3327 (1999).
[13]C. H. Ku, H. H. Chiang, and J. J. Wu, Chem. Phys. Lett. **404**, 132 (2005).
[14]M. C. Payne, M. Teter, D. C. Allan, and J. D. Joannopoulos, Rev. Mod. Phys. **64**, 1045 (1992).
[15]A. J. Read and R. J. Needs, Phys. Rev. B **44**, 13071 (1991).
[16]H. J. Monkhorst and J. D. Pack, Phys. Rev. B **13**, 5188 (1976).
[17]B. P. Zhang, N. T. Binh, K. Wakatsuki, Y. Segawa, Y. Kashiwaba, and K. Haga, Nanotechnology **15**, S382 (2004).
[18]B. Meyer and D. Mark, Phys. Rev. B **67**, 035403 (2003).
[19]S. W. Jung, W. I. Park, H. D. Cheong, G.-C. Yi, and H. M. Jang, Appl. Phys. Lett. **80**, 1924 (2002).
[20]K. Vanheusden, W. L. Warren, C. H. Seager, D. K. Tallant, J. A. Voigt, and B. E. Gnade, J. Appl. Phys. **79**, 7983 (1996).
[21]M. H. Huang, Y. Wu, H. Feick, N. Tran, E. Weber, and P. Yang, Adv. Mater. (Weinheim, Ger.) **13**, 113 (2001).
[22]R. Zimmermann, J. Cryst. Growth **101**, 346 (1990).
[23]I. A. Buyanova, W. M. Chen, G. Pozina, J. P. Bergman, B. M. Monemar, H. P. Xin, and C. W. Tu, Appl. Phys. Lett. **75**, 501 (1999).
[24]N. B. Chen and C. H. Sui, Mater. Sci. Eng., B **126**, 16 (2006).
[25]J. F. Sarver, F. L. Katnack, and F. A. Hummel, J. Electrochem. Soc. **106**, 960 (1959).
[26]R. D. Shannon, Acta Crystallogr., Sect. A: Cryst. Phys., Diffr., Theor. Gen. Crystallogr. **A32**, 751 (1976).